Chapter 14

The Scalable Design of Flapping Micro-Air Vehicles Inspired by Insect Flight

David Lentink, Stefan R. Jongerius, and Nancy L. Bradshaw

Abstract Here we explain how flapping micro air vehicles (MAVs) can be designed at different scales, from bird to insect size. The common believe is that micro fixed wing airplanes and helicopters outperform MAVs at bird scale, but become inferior to flapping MAVs at the scale of insects as small as fruit flies. Here we present our experience with designing and building micro flapping air vehicles that can fly both fast and slow, hover, and take-off and land vertically, and we present the scaling laws and structural wing designs to miniaturize these designs to insect size. Next we compare flapping, spinning and translating wing performance to determine which wing motion results in the highest aerodynamic performance at the scale of hummingbirds, house flies and fruit flies. Based on this comparison of hovering performance, and our experience with our flapping MAV, we find that flapping MAVs are fundamentally much less energy efficient than helicopters, even at the scale of a fruit fly with a wing span of 5 mm. We find that insect-sized MAVs are most energy effective when propelled by spinning wings.

14.1 Introduction

Recently, micro-air vehicles (MAVs) have gained a lot of interest of both aerospace engineers and biologists studying animal flight. Such small planes are of special interest because they have many promising civil and military applications: from inspection of buildings and other structures to silent and inconspicuous surveillance. These small sensor platforms with a wingspan of less than 10 in. can potentially be equipped with various micro-sensors ranging from multiple microphones and cameras to gas detectors. But how can one design such small planes best?

One major problem is aerodynamics. MAVs have a size and flight speed comparable to insects and small birds, which are much smaller and slower than airplanes. The aerodynamic effect of low speed and small size is quantified by the Reynolds number. The Reynolds number is the ratio of inertia and viscous stress in the flow and ranges roughly from 10 to 100,000 for insects to birds, and MAVs, whereas it ranges from 300,000 to 100,000,000 for airplanes. The low Reynolds number aerodynamics of MAVs is therefore more similar to that of flying birds and insects than that of airplanes. Only little is known about the aerodynamics in the low Reynolds number domain, which is studied mainly by biologists. Many engineers have therefore looked for biological inspiration for the design of their MAVs. Of special interest are insect-sized MAVs that can actually fly like insects using flapping wings: ornithopters. It is not widely known that several bird-sized, freely flying, ornithopters have been built and successfully flown even before Otto Lilienthal and the Wright brothers took off into the air with their, now, conventional airplanes. Ever since there have been few, but successful, amateur ornithopter enthusiasts that have developed many bird-sized ornithopters. The most successful predecessor of DelFly, a flapping MAV which we present here, is the AeroVironment Microbat, which could fly

D. Lentink (✉)
Experimental Zoology Group, Wageningen University, 6709 PG Wageningen, The Netherlands; Faculty of Aerospace Engineering, Delft University of Technology, 2629 HS Delft, The Netherlands
e-mail: david.lentink@wur.nl

D. Floreano et al. (eds.), *Flying Insects and Robots*,
DOI 10.1007/978-3-540-89393-6_14, © Springer-Verlag Berlin Heidelberg 2009

for 42 s [14]. An up-to-date historic overview of flapping MAVs can be found on www.ornithopter.org.

Developing a working insect-sized ornithopter that can both hover, fly fast and take off and land vertically like insects can remain, however, an open challenge. Not only because of small scale but also because we only know since roughly 10 years how insects can generate enough lift with their wings to fly [4, 3, 5, 18]. Biologists have found that a key feature that enables insects to fly so well is the stable leading edge vortex that sucks their wings upward, which augments both wing lift and drag. Building MAVs at the size of insects is even more challenging, because the critical components for successful flight cannot yet be bought at small enough size, low enough weight and high enough efficiency. Further, special production processes and design strategies are needed to build micro-flapping wings that function well at the length scale of insects. The ultimate dream of several engineers and biologists is to build a fruit fly-sized air vehicle.

Here we present an integrated design approach for micro-air vehicles inspired by insect flight that really fly and can be scaled from bird size to insect size.

14.2 The Scalable Wing Aerodynamics of Hovering Insects

To quantify if the aerodynamics of hovering insect wings are scalable from bird size to insect size we chose to study hovering flight, because it is the most power and lift demanding flight phase. Under hover conditions we measured the aerodynamic forces generated by a fruit fly wing model at Reynolds numbers (*Re*) of 110 (fruit fly sized), 1400 (house fly sized) and 14,000 (hummingbird sized). We performed these experiments with a robotic insect model at Caltech, RoboFly [5], in collaboration with Michael Dickinson (for details and methods, see [11]). The RoboFly setup consists of a tank filled with mineral oil in which we flapped a fruit fly-shaped wing using both measured and simplified fruit fly kinematics. The simplified fruit fly kinematics consists of sinusoidal stroke and filtered trapezoidal angle of attack kinematics. The stroke amplitude of 70° (half the full amplitude defined in [2]) is based on the measured kinematics of six slowly hovering fruit flies [6]. The angle of attack amplitude was varied from 0° to 90° in steps of 4.5°, which encloses the full range of angle of attacks relevant for the flight of flies (and other insects). The lift and drag measurements at fruit fly scale, $Re = 110$, show that flapping fruit fly wings generate roughly twice as high lift coefficients as translating ones (lift coefficient is equal to lift divided by the product of the averaged dynamic pressure and wing surface area; the drag coefficient is similarly defined). RoboFly force measurements using actual kinematics of slow hovering fruit flies reveal that fruit flies indeed generate much more lift by flapping their wing than generated when the same wing is simply translated, like an airplane, Fig. 14.1. The force coefficients measured for fruit fly kinematics overlap with the lift–drag coefficient polar generated with the simplified fruit fly flap kinematics, Fig. 14.1.

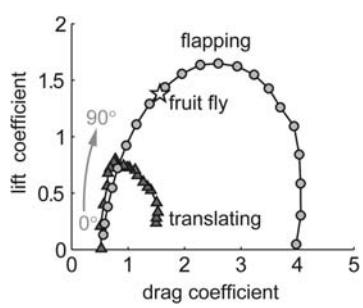

Fig. 14.1 Flapping fly wings generate more lift than translating fly wings. Stroke-averaged lift–drag coefficient polar of a translating (*dark grey triangle*), simple flapping (*light grey circles*) and realistically flapping (*star*) fruit fly wing at $Re = 110$. The angle of attack amplitude ranges from 0° to 90° in steps of 4.5° [11]

The elevated lift and drag forces generated by a fruit fly wing are due to a stably attached leading edge vortex (LEV) on top of the wing, which sucks the wing upward, Fig. 14.2. A stable LEV that explains the elevated lift forces generated by hovering insects was first found for hawkmoths [3]. Dickinson et al. [5] measured the actual unsteady forces generated during a flap cycle of a fruit fly wing, which showed that indeed much, up to 80%, of the total lift can be attributed to the 'quasi-steady' lift contribution of the stable leading edge vortex. To test if the aerodynamics of flapping fly wings is indeed scalable we flapped the same wing, using the same kinematics, in less viscous oil (house fly scale, $Re = 1400$) and finally water (humming bird scale, $Re = 14{,}000$), which is even less viscous. We found that the lift–drag coefficient polars did not change much, the main effect we found is

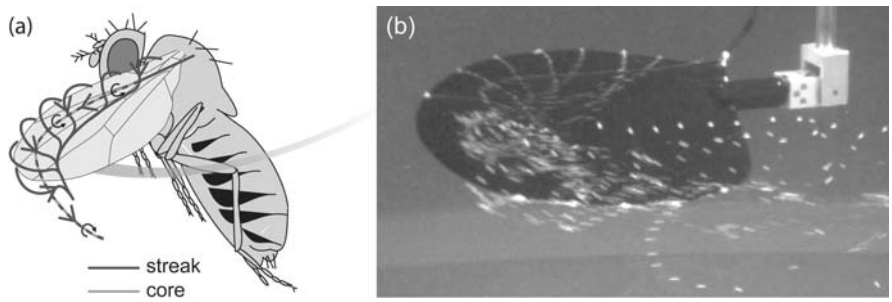

Fig. 14.2 (**a**) Cartoon of the leading edge vortex that is stably attached to the wing of a fruit fly. (**b**) Flow visualization of this stable LEV on a fruit fly wing at Re=110. Visible are air bubbles that swirl into the LEV after they were released from the leading edge of a fruit fly wing immersed in a tank with mineral oil [11]

that the lift coefficients generated at fruit fly scale are a bit smaller and the minimum drag coefficient a bit higher, due to viscous damping Fig. 14.3. This shows that the aerodynamic forces generated by flapping fly wings can be estimated well across this whole Reynolds number range using the coefficients measured at either $Re = 110$, 1400 or 14,000, multiplied by the average dynamic pressure and wing surface area that correspond with the scale of interest (average dynamic pressure is calculated using a blade element method [2]).

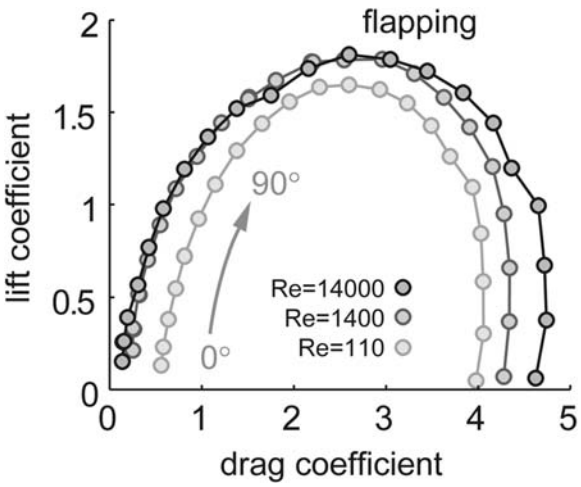

Fig. 14.3 The forces generated by a flapping fly wing depend weakly on Reynolds number. Stroke-averaged lift–drag coefficient polar of a model flapping fruit fly wing (*light grey circles*) at $Re = 110$, 1400 and 14,000. The angle of attack (amplitude) ranges from 0° to 90° in steps of 4.5°. The lift–drag coefficient polars only weakly depend on Re, especially for angles of attack close to 45°, which correspond approximately with maximum lift. The polars at $Re = 1400$ and 14,000 are almost identical [11]

14.3 Design Approach: Scale a Flapping MAV That Works Down to Smaller Sizes

Model airplane enthusiasts have demonstrated that small, lightweight airplanes can be built with wingspans that range from 70 to 10 cm, of which the lightest weigh around 1 g (e.g. www.indoorduration.com). The biggest challenge might be the availability of high-performance micro-components that build up the flight system: micro-radio controllers (RC), actuators, motors, batteries, etc. (see the extensive list of suppliers in Appendix 1). Keeping in mind that both aerodynamics and structure are not limiting to scaling ornithopters, it is advantageous to develop a relatively large, well-flying ornithopter inspired by existing ornithopter designs and insect flight. This scale should be chosen such that the required electronic and mechanical components are both commercially available and affordable. An artist impression of this approach is shown in Fig. 14.4. Based on this approach we first designed and built DelFly, a 35 cm span (22 g) flapping 'MAV'. It can fly both fast and perform slow hovering flight for maximal 15 min, while streaming video (2005). Next we scaled the DelFly design down to 28 cm span (16 g), DelFly II (2006), which can take off and land vertically. DelFly II can hover for 8 min and fly fast for 15 min, while streaming video. Recently Nathan Chronister scaled the DelFly to 15 cm span (3.3 g); this model can both hover and fly loopings. The group of Yoshiyuki Kawamura has made the next step in an earlier phase (2006–2007) and scaled down the DelFly design to 10 cm span (2.3 g) which flies for a couple of minutes [8]. This 10 cm span ornithopter is the first successful insect-sized flapping MAV.

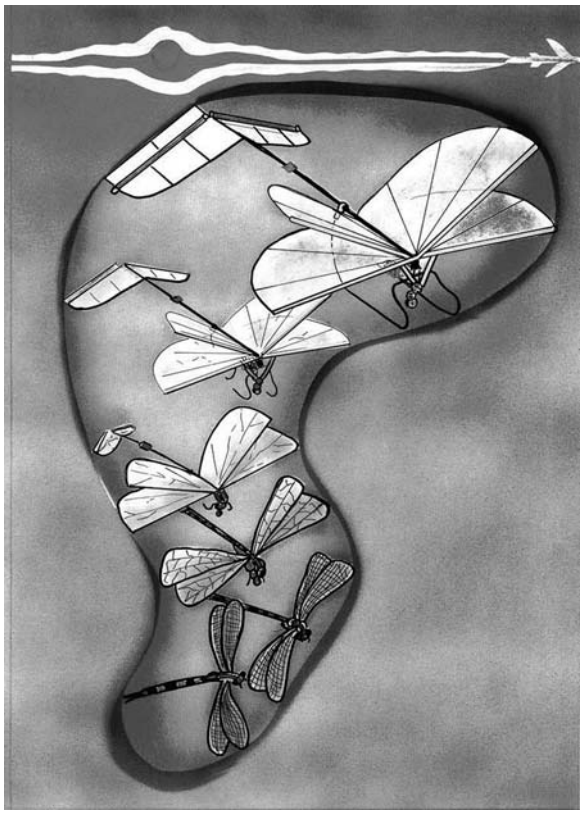

Fig. 14.4 Artist impression of micro-aerial vehicle design inspired by insect flight

14.4 DelFly: A Flapping 'MAV' That Works

The aim of the DelFly project was to design a stable, radio-controlled, flapping MAV that could fly for 15 min and function as a sensor platform. The DelFly mission was to detect a person walking with a red suitcase. For this DelFly is equipped with an onboard colour camera, of which the images were streamed live to a base station with situation awareness software. The team consisted of 11 bachelor students of Delft University of Technology supervised by scientists and engineers from Wageningen University, Delft University of Technology and Ruijsink Dynamic Engineering.

To kick start the project the students started out with flight testing three existing rubber-band-powered ornithopter designs: a monoplane, biplane and tandem design, Fig. 14.5. The fight test procedures are described in Appendix 2. Although these ornithopters cannot be considered MAVs, because they fly uncontrolled and too briefly, they have two big advantages. First, they are inherently stable designs. Second, the in-flight torque of the rubber band can be determined using a torque meter constructed of a thin, calibrated, piano-steel wire, and the windings in the rubber band can be counted easily; the result is illustrated in

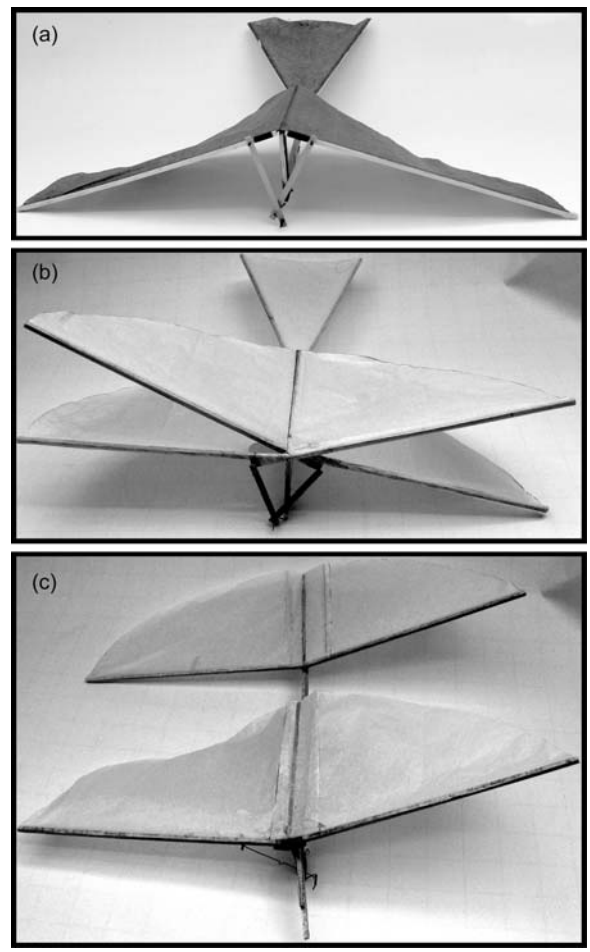

Fig. 14.5 Three different rubber-powered ornithopter configurations flight tested for the design of DelFly. (**a**) Falcon, a monoplane ornithopter available at www.ornithopter.org. A single pair of wings is powered by a rubber band. (**b**) Luna, a biplane ornithopter available at www.ornithopter.org. Its two wings form a cross; the two lower legs of the cross are actuated. As a result the upper and lower left wings flap towards and away from each other (same for the right wing). (**c**) Tandem wing ornithopter, custom built inspired by an existing Swedish design. The two tandem wings flap in anti-phase, the front wing is actuated and the hind wing flaps 180° out of phase in reaction to this. The front wing is connected to one side of the rubber band and the hind wing is connected to the fuselage to which we attached the other side of the rubber band

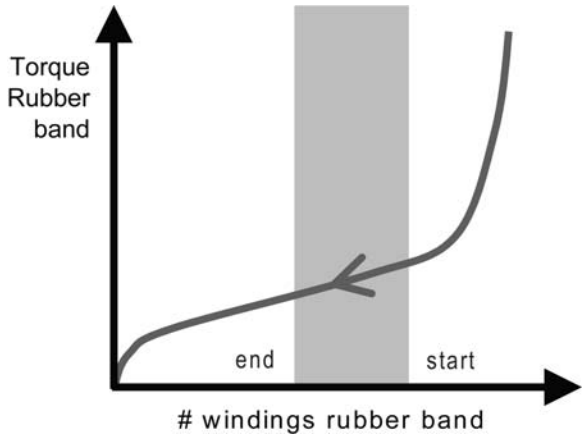

Fig. 14.6 Rubber band torque vs. number of windings. After putting in a certain number of winds into a rubber band (e.g. 1000) it starts to unwind at the right side of this graph at peak torque. We first let the rubber unwind such that the torque flattens off and then start performing a test flight. Knowing the start and end torque and the number of windings in the rubber band (counted during (un)winding) the in-flight torque can be estimated well, especially with the movies we made of every flight, for which we used the recorded flapping sound of the ornithopter to determine its flap frequency. High-quality rubber band is the key to good flight performance and useful measurements: www.indoorduration.com

Fig. 14.6. During the flight test of the three ornithopter configurations we measured the mass, torque (at the start and end of flight), flap frequency (audio data) and average flight velocity (video data). Finally we estimated the rocking amplitude at the front of the ornithopter (video data), where we planned to fit the camera. Using torque and flap frequency we computed the average power consumption. The measured and calculated flight variables can be found in Table 14.1.

Based on the measurements we found that it was most difficult to trim the tandem design such that it flew well, and we therefore eliminated this configuration. The two competing configurations were the monoplane and biplane configurations. The monoplane appeared to be the most efficient flyer, but flew at relatively high speed and rocked significantly. Therefore, we chose the slower biplane configuration which rocked least, which is critical for a camera platform. Having reliable performance estimates is critical for sizing the electronic components, actuators, motor, gearbox and battery. For the sizing we used simple scaling laws to obtain realistic torques, frequencies, power consumption and flight speed estimates for an arbitrary size, using the measured data in Table 14.1. In our scaling we assume that the flight path is the same for both the original (indicated with '1') and the newly scaled ornithopter (indicated with '2'). To determine the new horizontal velocity U_∞ we use the fact that lift equals weight during horizontal flight as follows:

$$mg \propto C_L 1/2\rho U_\infty^2 S \rightarrow U_{\infty,2} = U_{\infty,1}\left(\frac{m_2}{m_1}\frac{S_1}{S_2}\right)^{0.5}, \tag{14.1}$$

where m is the mass, C_L the lift coefficient which we assume to be independent of Reynolds number (Fig. 14.3), ρ the air density (constant), U_∞ the forward flight velocity of the ornithopter and S the wing surface area. We use the proportional instead of equal sign, because the proportionality remains valid for other flight conditions such as climbing and turning. The required power P is proportional to weight times speed (because drag scales with weight) as follows:

$$\begin{aligned} P \propto mgU_\infty \rightarrow P_2 &= P_1 \frac{U_{\infty,2}}{U_{\infty,1}}\frac{m_2}{m_1} \rightarrow P_2 \\ &= P_1\left(\frac{m_2}{m_1}\right)^{1.5}\left(\frac{S_1}{S_2}\right)^{0.5}, \end{aligned} \tag{14.2}$$

where g is the gravity constant. To determine the flap frequency we need to know how forward speed U_∞ and the flap frequency f are related; for this we assume that the advance ratio J [2, 12] of the ornithopter remains constant:

Table 14.1 Flight test results of the three ornithopter configurations

Variable Unit	m g	S m^2	b m	T Nm	f Hz	V m/s	P W	Rocking mm
Monoplane	6.7	0.043	0.41	0.0075	3.7	1.7	0.18	80
Biplane	8.0	0.074	0.35	0.0064	6.7	1.3	0.28	± 0
Tandem	10.9	0.066	0.35	0.013	7.9	1.5	0.66	–

The tandem configuration was difficult to trim and did not fly well as a result. We averaged over flight tests during which we judged the ornithopter to be trimmed well; fly stable. The variables are as follows: m, mass; S, total wing area; b, wing span; T, torque needed to drive the wings; f, flap frequency; V, flight speed; P, required power; rocking, rocking amplitude at the front of the ornithopter

$$J = \frac{U_\infty}{4f\Phi_0 R} = const \rightarrow f_2 = f_1 \frac{U_{\infty,2}}{U_{\infty,1}} \frac{\Phi_{0,1} R_1}{\Phi_{0,2} R_2} \rightarrow f_2$$
$$= f_1 \left(\frac{m_2}{m_1} \frac{S_1}{S_2} \right)^{0.5} \left(\frac{\Phi_{0,1} R_1}{\Phi_{0,2} R_2} \right), \tag{14.3}$$

where Φ_0 is the stroke amplitude in radians (half the total amplitude defined in [2]) and R the single wingspan (radius). If we assume that the stroke amplitude is constant, which is true for isometric scaling, this relation becomes straightforward. What if measurements are performed for hovering flight when $U_\infty = 0$? To scale both hovering and forward flight continuously we suggest to use the wing tip speed V in Eqs. (14.1) and (14.2) instead of U_∞, which is within good approximation [10, 12]:

$$V \approx \sqrt{U_\infty^2 + (4f\Phi_0 R)^2}. \tag{14.4}$$

Based on the calculated power and the specs of the battery pack we can now calculate the average motor current as follows:

$$I_2 = \frac{P_2}{V_{\text{LiPo}}}. \tag{14.5}$$

where I_2 is the motor current of the newly scaled ornithopter and V_{LiPo} the voltage of the lithium-polymer battery pack. The total flight time in seconds can now be estimated as follows:

$$t_2 = 3.6 \frac{C_{\text{LiPo}} V_{\text{LiPo}}}{P_2}, \tag{14.6}$$

where C_{LiPo} is the capacity of the lithium-polymer battery pack (mA h). Based on the required power, the voltage of the battery pack and the flap frequency, a motor can now be selected (see www.didel.com for pager motor selection charts). Based on the rpm of the selected motor $RPM_{\text{motor},2}$, the required gearbox ratio red_2 is as follows:

$$red_2 = \frac{RPM_{\text{motor},2}}{60 f_2}, \tag{14.7}$$

Using a spreadsheet and Eqs. (14.1)–(14.17) the 'components off the shelf' (COTS) are chosen which means components are bought as light and small as currently available in retail. We illustrated the main components chosen to build DelFly in Fig. 14.7 (these are representative, not actual, photos). In 2005 these were the most lightweight components available (see the extensive list of suppliers in Appendix 1). The weight, power consumption and other performance indices of these components determined the smallest possible dimensions of DelFly at which it could fly for 15 min and stream live video.

The main component of DelFly is the battery. In order to choose a suitable battery two criteria are important: the capacity and the maximum discharge rate. The first parameter, the required capacity, is determined by the required flight duration and the power consumption of the electric systems. The second, the maximum required discharge rate, is determined by the maximum power required by the total electrical system. The latter is a problem with most lightweight batteries. Therefore, we selected a battery with a least power to weight ratio and a sufficient maximum discharge rate. The lightest available battery fulfilling these requirements is a 140 mA h lithium-polymer battery as seen in Fig. 14.8. It could discharge up to five times its capacity, 700 mA, which is enough.

The biggest energy consumer is the motor that powers the flapping wings of DelFly. We chose a brushed pager motor, because of its availability. Brushless motors are more efficient, but the available motors cannot handle the periodic loading due to the flapping wings. The motor drives a gearbox (see Fig. 14.7) to reduce the RPM of the motor to match the required flapping frequency of the wings. A dedicated crankshaft, conceptually the same as that of the Falcon biplane, connects the gearbox to the two lower legs of the X-wing and drives both lower wings in phase. The left lower wing is directly connected to the right upper wing and vice versa. Therefore both sides of the X-wing flap synchronously towards each other and away from each other (buying the actual kits helps to get a good three-dimensional picture of this system). We re-designed the flapping mechanism itself using the freely available Java software at www.ornithopter.org/software.shtml.

For controlling DelFly we used standard model aircraft RC radio equipment. The remote control sends control signals to DelFly's onboard receiver (see Fig. 14.7). This in turn translates the control signal to a power signal to the coil actuators (see Fig. 14.7), which we connected to the control surfaces.

DelFly also has a camera onboard for two reasons. First, a camera is a useful sensor to obtain images of its surrounding. Second, the camera in combina-

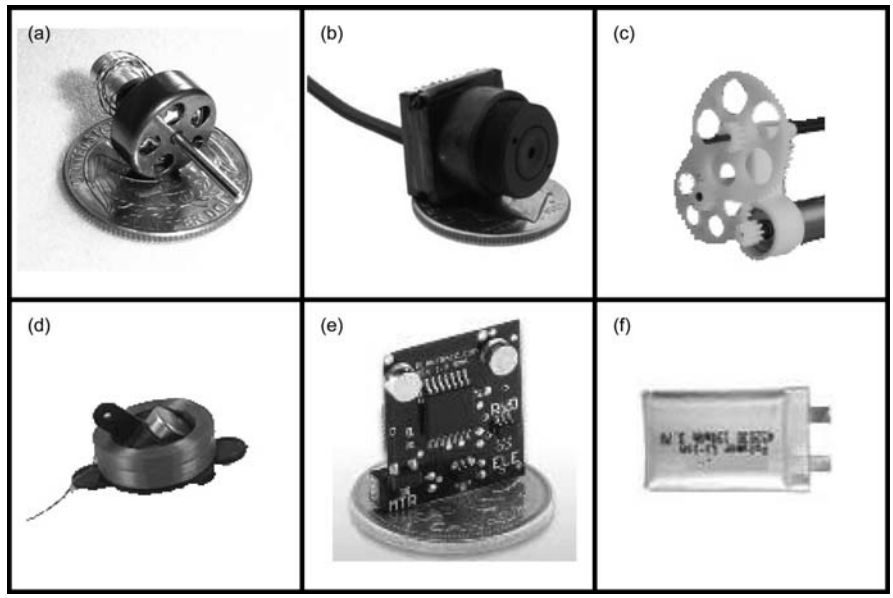

Fig. 14.7 Illustration of the main components of DelFly (and DelFly II): (**a**) brushless electric motor (www.bsdmicrorc.com; modified for use on DelFly II); (**b**) colour camera (www.misumi.com.tw); (**c**) plastic gear box (www.didel.com); (**d**) micro-actuators (www.bsdmicrorc.com/); (**e**) receiver (www.plantraco.com); and (**f**) lithium-polymer battery (www.atomicworkshop.co.uk)

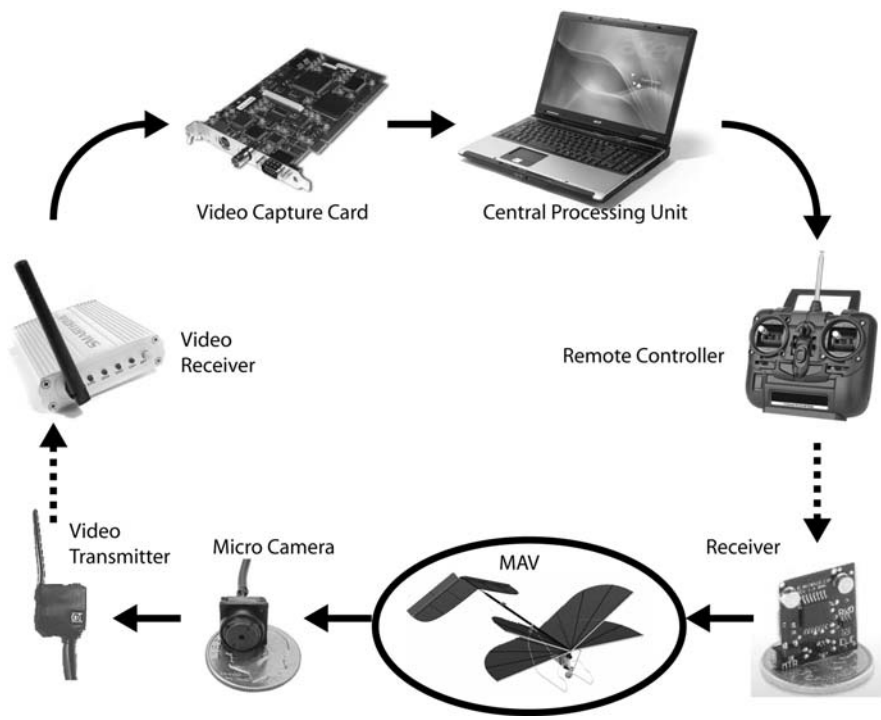

Fig. 14.8 Control loop for vision-based awareness of DelFly

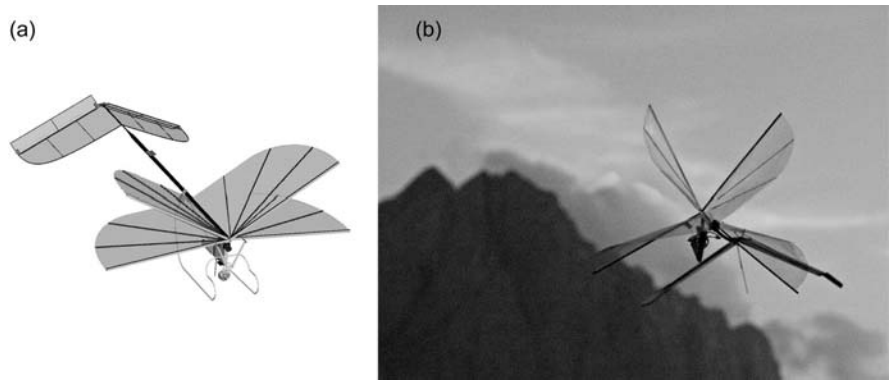

Fig. 14.9 Three-dimensional CAD drawing of the DelFly design (**a**) and DelFly flying in the European Alps (**b**)

tion with dedicated vision software can be part of the control loop. DelFly has a camera onboard that sends video signals via the transmitter to the receiver on the ground. This signal enters a central processing unit, usually a personal computer or laptop, via its video card. Dedicated software is installed on the central processing unit, which analyses the video signal to detect objects like a red suitcase or compute the optical flow. Based on the image analysis the base station then sends updated control signals to DelFly via the RC radio to the receiver on board of DelFly. This continuous control loop for vision-based awareness is illustrated in Fig. 14.8.

All the components combined resulted in the design shown in Fig. 14.9a. The combined mass of all (electronic) components is approximately 12.5 g. To carry this load and bear the corresponding aerodynamic and inertial loads we designed a lightweight structure of approximately 4.5 g. The structure consists primarily of carbon fibre rods. The wings leading edge spars are made of a balsa–carbon (unidirectional) sandwich that is much less stiff in flight direction than in flap direction. This stiffness asymmetry is essential to make the wing deform well aero-elastically. The wing is covered with transparent Mylar foil of 7 g/m^2. We used cyano-acrylate for gluing carbon–carbon, epoxy for gluing carbon–balsa and transparent Pattex hobby glue, diluted 1:1 with acetone, for gluing carbon–Mylar.

DelFly turned out to be an easy to control and very stable flapping MAV, Fig. 14.9b. Its main drawback is that it can get into a spiral dive when turning too tightly and too fast at too low angle of attack, because the actuators are slightly underpowered for this flight condition (finding strong and light enough actuators remains a challenge for MAV design).

14.5 DelFly II: Improved Design

After designing and building DelFly within a student project we professionalized the DelFly design and better quantified its aerodynamic performance. For this we were supported by TNO (The Netherlands), which resulted in the DelFly II design, shown in Figs. 14.10 and 14.11. DelFly II weighs about 14 g without payload and 17 g with payload, a camera and video transmitter. The wingspan is reduced from 35 cm to 28 cm and its length is reduced from 40 cm to 28 cm, such that it fits in a 30 cm diameter sphere. The most important difference between DelFly and DelFly II is its symmetric driving mechanism and the custom-refitted brushless motor. This brushless electric motor has enough power to enable DelFly II to vertical take-off and landing, shown in Fig. 14.12. The motors' efficiency of roughly 60% enables it to fly longer than normal, using a pager motor instead will still allow DelFly II to take off and land vertical and hover at the cost of some flight duration. The brushless motor we used had to be refitted with different windings, magnet configuration and controller software such that it could cope with the highly varying drive torque of the flapping wings. Note that brushed pager motors do not need special modifications to drive a flapping wing and are therefore a time efficient and inexpensive solution (see the extensive list of suppliers in Appendix 1).

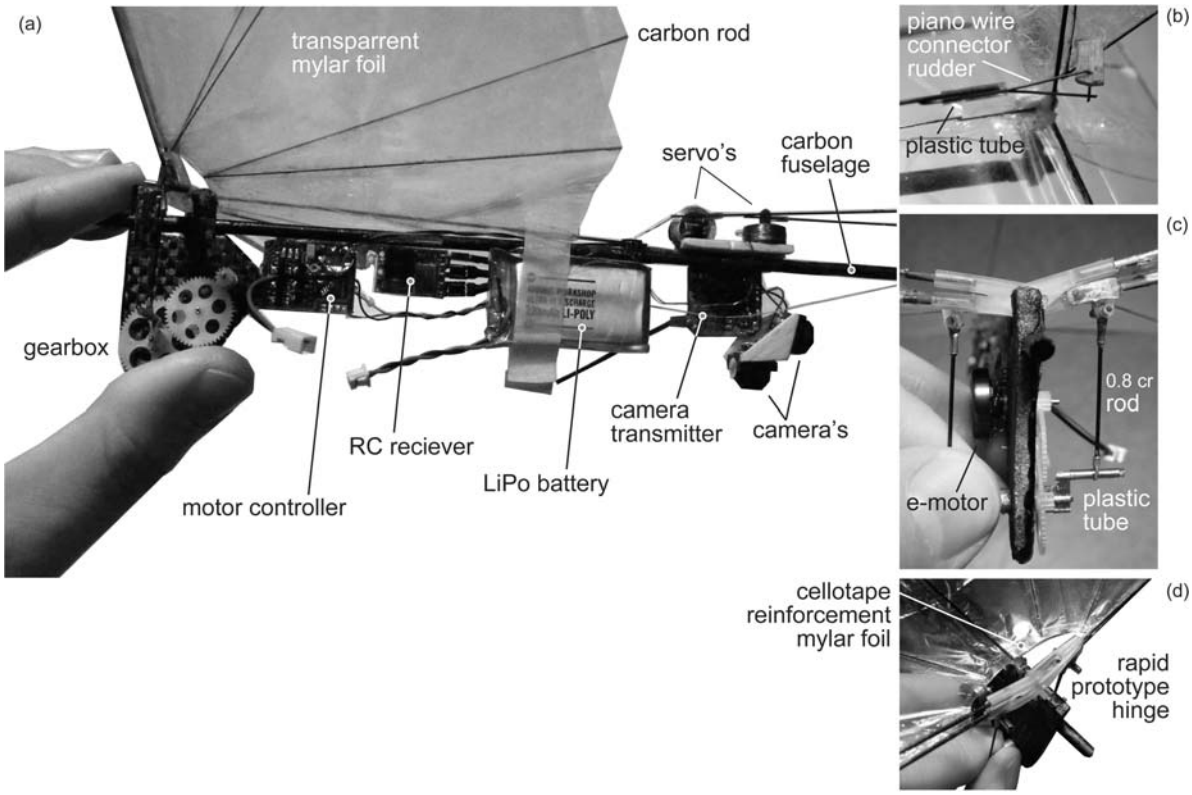

Fig. 14.10 Detailed photos of DelFly II. (**a**) Main components of DelFly II. The front part of the carbon fuselage is a sandwich of carbon cloth (65 g/m^2) with a Rohacell core (lowest density available). The transparent Mylar foil weighs 7 g/m^2. (**b**) Rudder connection mechanism for the controls. (**c**) Brushless electric motor (e-motor) and the symmetric driving mechanism of both lower legs of the X-wing. The rotary motion of the gears is converted into a translating motion through the carbon fibre rods (cr-rods) that are fitted with a small bearing consisting of a flattened brass rod with a hole drilled in it. (**d**) Wing root with cellotape reinforced Mylar film and rapid prototype wing hinge (www.quickparts.com)

14.6 DelFly II: Aerodynamic Analyses

Insects have limited control over the wing shape, because their muscles stop at the base of their wings. The aero-elastic wings of insects are therefore thought to be passively stabilized. The aero-elastic wings of ornithopters like DelFly have passively stabile aero-elastic wings too, which deform strongly under loading. But what forces mediate DelFly's wing deformation, aerodynamic loading or wing inertia? And how much power is lost with accelerating and decelerating a flapping wing continuously? What flap angles result in the best hover performance, and how high are the lift coefficients generated by a strongly deforming aero-elastic wing? The answers to these questions are likely to be as relevant for optimizing DelFly as they are for getting insight into the aerodynamics of aero-elastic insect wings.

Based upon the coefficient that we measured for DelFly under hovering conditions, which is around 2, we believe that DelFly employs at least two of the high-lift mechanisms that are found in insect flight. First we think that DelFly creates a stable leading edge vortex (Fig. 14.2), like the AeroVironment Microbat [14]. Second we think DelFly benefits from the clap and fling mechanism of aero-elastic wings, which is utilized by small insects and butterflies [17]. The wings of DelFly clap and fling when the upper and lower wings come together as the X-wings close. The peeling motion of the aero-elastic DelFly wings resembles the wings of butterflies during take-off, Fig. 14.13. First the wings 'clap' together at the 'start' of the flap cycle, at 0%, after which they 'peel' apart at 12.5% through

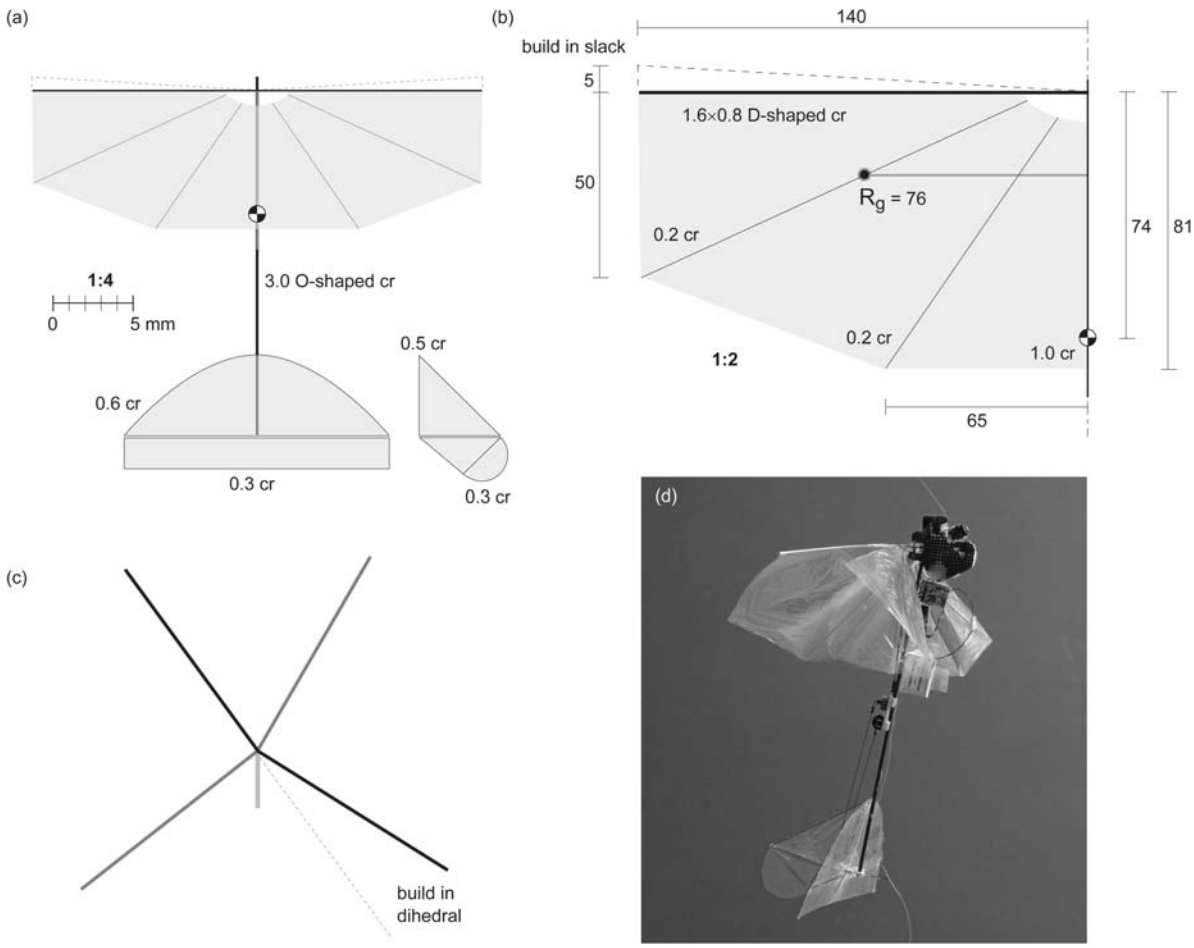

Fig. 14.11 Dimensions and building material of DelFly II. All the above are drawn to scale and angles are realistic: top view (**a**), wing dimensions (**b**) and build in dihedral (**c**). Note that *cr* stands for carbon fibre rod, whenever available we used hollow carbon rods. All carbon fibre components are available at www.dpp-pultrusion.com. (**d**) DelFly II in hovering flight, note that this is a slightly different model than shown in Fig. 14.10. Photo credit: Jaap Oldenkamp. Not shown is the X-shaped landing gear of DelFly II, build out of the leading edge carbon rods of the horizontal and vertical rudder. The landing X-rods are pulled together with two thin wires (e.g. nylon or Kevlar) and as a result they bend. The base of the landing gear has smaller dimensions than the wing span (dimensions are not very critical)

37.5% of the flap cycle. The clap and fling is essentially a combination of two independent aerodynamic mechanisms that should be treated separately. First during the clap the leading edges of the wing touch each other before the trailing edges do, progressively closing the gap between them. Second during the fling the wings continue to pronate by leaving the trailing edge stationary as the leading edges fling apart. A low-pressure region is supposedly generated between the wings and the surrounding fluid rushes in to occupy this region. This initializes the build up of circulation [17]. Experiments of Kawamura et al. [8] with a 10 cm span DelFly biplane model and a similar monoplane model showed that the clap and fling indeed increases thrust up to roughly 50%. The thrust–power ratio, a measure of efficiency, is also roughly 50% higher for the biplane configuration. Another explanation as to why insects might clap and peel their wings is that they simply try to maximize their stroke amplitude to maximize wing lift (for the same flap frequency). The lift force is proportional to velocity squared and therefore amplitude squared; maximization of the stroke amplitude will therefore significantly enhance the total flight forces [17].

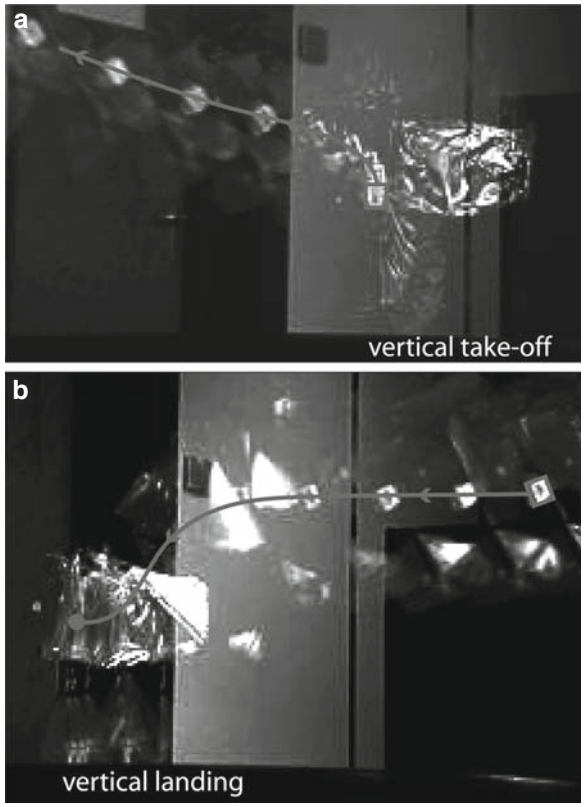

Fig. 14.12 Compilation of video images that illustrate the vertical take-off (**a**) and vertical landing (**b**) capabilities of DelFly II. The clearly visible *light square* is the reflective battery pack (LiPo)

14.6.1 DelFly Models Used for Aerodynamic Measurements

We studied the aerodynamic performance and aeroelastic deformation of DelFly II wings to maximize its lift and minimize its power consumption in hovering flight, the most power-consuming flight mode. These studies were performed at Wageningen University in collaboration with Delft University of Technology [1]. For these studies two DelFly II models were used:

DelFly IIa, powered by a strong brushed motor (simplified aluminium construction). This model was used for high-speed camera imaging

DelFly IIb, powered by a 3.5 V brushless motor of which the frequency is controlled by varying the current (realistic carbon fibre and plastic construction). This model was used for all except one performance measurement. We used a brushed motor for the performance analysis shown in Fig. 14.15, because it allowed us to test for higher flap frequencies.

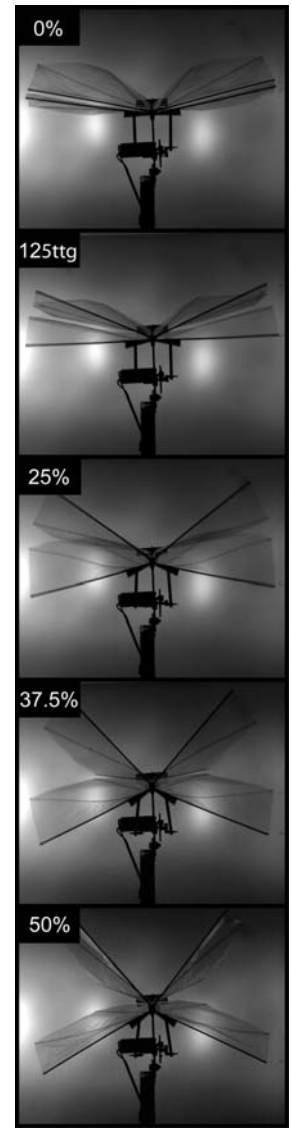

Fig. 14.13 High-speed video image sequence of the clap and fling of DelFly II wings in air at 14 Hz and 30° flap angle. The images are snapshots starting at the beginning of upstroke up to the start of the downstroke: 0%, 12.5%, 25%, 37.5% and 50% of the flap cycle

Figure 14.14a shows the DelFly IIb model mounted on a six-component force transducer. This transducer is capable of accurately measuring forces and torques (i.e. moments) in three directions with a resolution of

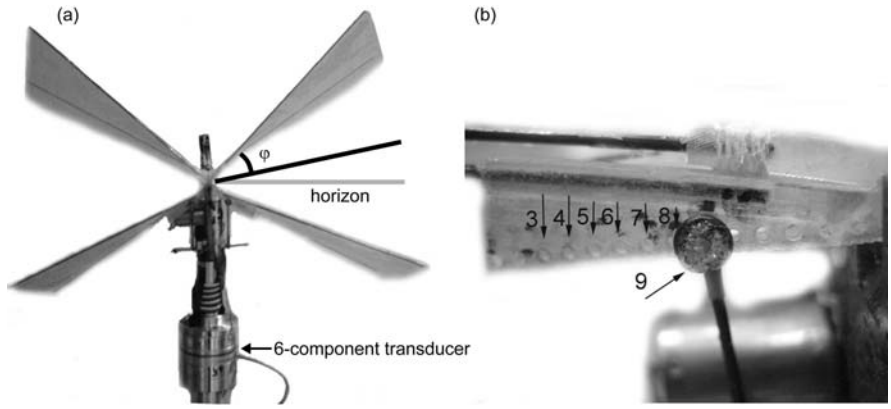

Fig. 14.14 (**a**) DelFly IIb mounted on the six-component transducer, ϕ indicates the flap angle. The *oblique line* indicates the wing position at the start of a flap cycle (upstroke) when the leading edge of the wing is at maximum deflection, i.e. 50% of the flap cycle, where the downstroke starts. (**b**) Wing hinge with different drive-rod positions that result in the different flap angles for which we measured the hover performance of DelFly

Table 14.2 Flap angle as a function of flap angle position. The final design of DelFly II has an even larger flap angle, for which special wing hinges were designed

Flap angle position	ϕ
3	17.5°
4	19.5°
5	21.5°
6	24°
7	27°
8	30°
9	36°

approximately 0.5 g. The flap angle is indicated by ϕ. Different flap angles are obtained by connecting the drive rod to the different connection points at the wing's hinge, shown in Fig. 14.14b, the actual values are given in Table 14.2.

14.6.2 Lift as a Function of Flap Frequency at a Constant Flap Angle of 36°

We found that lift increases linearly with wing beat frequency between 14 and 20 Hz at a constant flap angle of 36°, Fig. 14.15. This flap angle was chosen because this flap angle most closely resembles the flap angle of DelFly in flight. The frequency range was determined by the maximum power output of the *brushed* motor fitted on DelFly II B. Figure 14.15 shows that this model needs to flap at a frequency of 20 Hz to lift the payload (total mass 17 g) during hovering and a frequency of 17.2 without payload (14 g). The final DelFly II design flaps at lower frequencies, because it has a larger flap angle than we could test with the

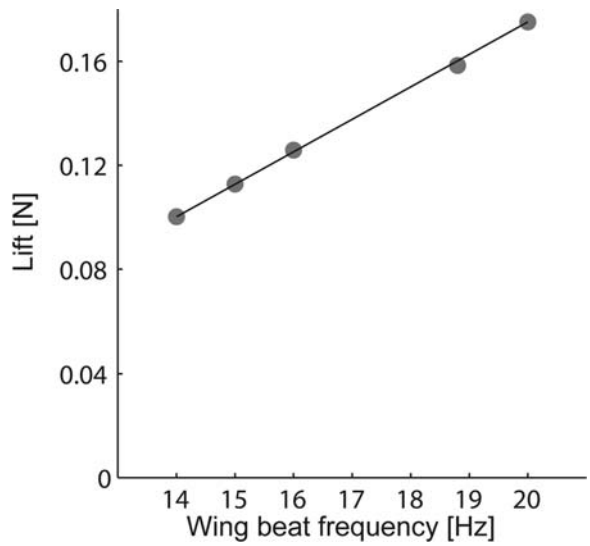

Fig. 14.15 Lift vs. wing beat frequency at a constant flap angle of 36°. The *line* indicates the linear trend, whereas a quadratic trend is expected (lift is proportional to frequency squared). We think the linear trend with increasing frequency results from the increasingly higher lift forces that deform the wing more and more, and therefore reduce the angle of attack of the wing, which lowers lift force (because lift is proportional to the angle of attack)

here-used hinge. Note that the net wing speed is proportional to flap angle times frequency and that this product is roughly the same for our DelFly IIb and the final design, because both operate at similar lift coefficients.

14.6.3 Lift and Power as a Function of Flap Angle at a Flap Frequency of 14 Hz

Both lift and power increase with flap angle, but the more important lift over power ratio reaches a plateau, Fig. 14.16. The lift over power ratio is a measure of how effectively DelFly generates lift. The required power measurements include the aerodynamic power as well as the power needed to drive the motor, the drive train and overcome the inertia of the complete mechanism (accelerate and decelerate it). Both the lift and the required power increase with flap angle, because wing speed increases with flap angle (at constant frequency). Theoretically lift is proportional to the flap angle squared, and aerodynamic power to the flap angle cubed. Because the experiment is carried out at constant flap frequency the flap velocity, and therefore wing lift, increases significantly with flap angle. The increasing lift deforms the aero-elastic wing increasingly more. These significant deformations might explain why the lift over power ratio is not proportional to the inverse of flap angle, predicted by theory. The measurements suggest that the most efficient flap angle is higher than 30° for DelFly II flapping at 14 Hz. The Reynolds number in these experiments varied from 3700 to 7600. Based on Fig. 14.3 we do not expect that this difference in Reynolds numbers affects the wings' lift coefficients much.

The dimensionless lift and power coefficients of DelFly II flapping at 14 Hz are shown in Fig. 14.17. The lift coefficients have high values, $C_L = 1.8$–2.5, compared to the lift coefficients of translating wings at similar Reynolds numbers of which the maximum lift coefficient is approximately 1. The power coefficients are calculated by dividing power by the product of dynamic pressure, wing speed and wing surface area using a blade element method [2]. It is striking that these coefficients are an order of magnitude greater than the force coefficients. Based on scale arguments we expected that both coefficients are of order 1, $O(1)$. An explanation for this inconsistency might be in the fact that we used total power instead of aerodynamic power. In order to determine aerodynamic power we had to separate it from the power needed to drive the motor, the drive train and overcome inertial forces. We determined the aerodynamic power by measuring the required power under vacuum conditions and subtracting that power from the power needed to flap at the same frequency in air. For these experiments we designed and built a custom vacuum chamber with a minimum pressure of 10 Pa.

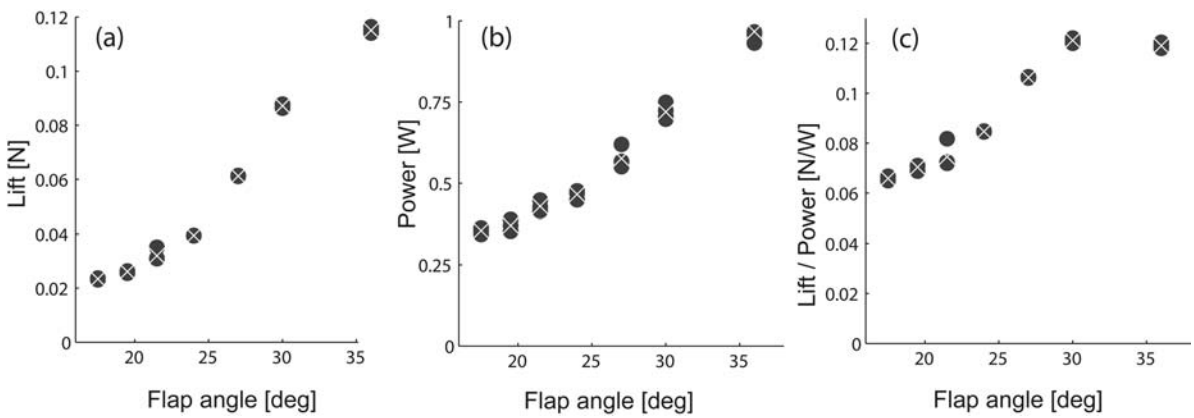

Fig. 14.16 Lift, power and efficiency of DelFly: (**a**) lift vs. flap angle at a constant wing beat frequency of 14 Hz; (**b**) power vs. flap angle at a constant wing beat frequency of 14 Hz; and (**c**) the ratio of lift to power vs. flap angle at a constant wing beat frequency of 14 Hz. The lift–power ratio is a measure of 'efficiency'. The *dots* give the results of the individual measurements per sequence and the *crosses* denote the mean value of the four runs

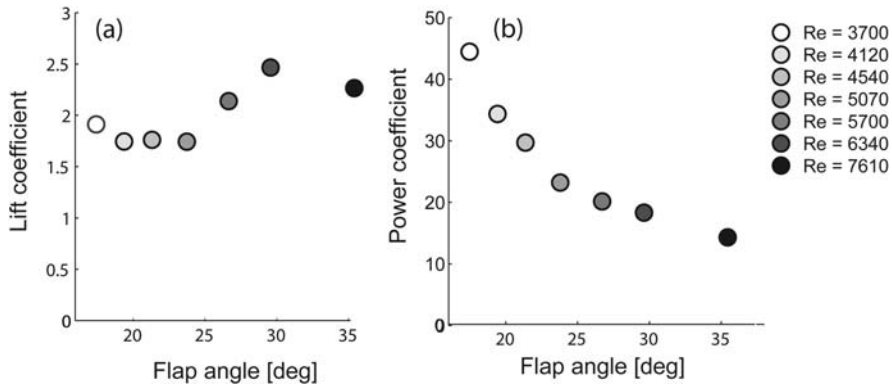

Fig. 14.17 Lift (**a**) and power (**b**) coefficients vs. flap angle at a constant wing beat frequency of 14 Hz. Power coefficients vary much more with flap angle than lift coefficients

14.6.4 Power Requirement and Wing Deformation in Air Versus Vacuum

The power losses of a flapping wing range from roughly 80% at a flap angle of 24° to 50% for a flap angle of 36°. To isolate the aerodynamic power, the power measured in near vacuum was subtracted from the power measured in air: $P_{aero} = P_{air} - P_{vac}$. We plotted the aerodynamic power as a percentage of total power as a function of flap frequency in Fig. 14.18. The results suggest that the power losses of DelFly are strongly dependent on the flap angle, but not so much on frequency. The larger flap angle results in the highest percentage of aerodynamic power, which partly explains why a large flap angle results in high flap performance, Fig. 14.16c. If we correct the power coefficient for a power loss of 80% at a flap angle of 24° and 50% at 36°, we obtain power coefficients of approximately 5 and 7.5 which are much closer to the values found for flapping fruit fly wings of 2–4 at similar angles of attack in Fig. 14.3. The remaining differences can still be explained by mechanical losses, because we were unable to correct for the effect of variable motor efficiency. The much lower torque in vacuum can drastically alter the efficiency of the brushless motor, we hope to better quantify this in a future study.

Finally we wanted to know how inertial versus aerodynamic forces deform the aero-elastic wing of DelFly. Using the vacuum chamber we made high-speed video images of the flapping foil in vacuum and air, Fig. 14.19. The wings deformation is signif-

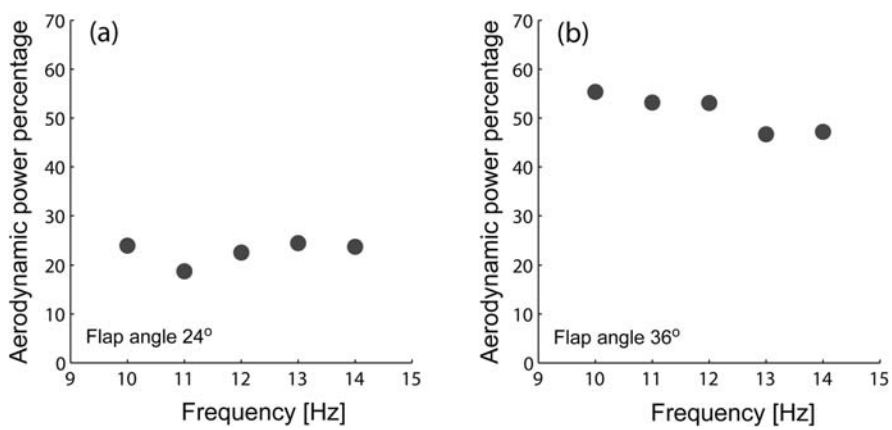

Fig. 14.18 Percentage of aerodynamic power compared to total power increases with flap angle and depends weakly on wing beat frequency: (**a**) flap angle of 24° and (**b**) flap angle of 36°

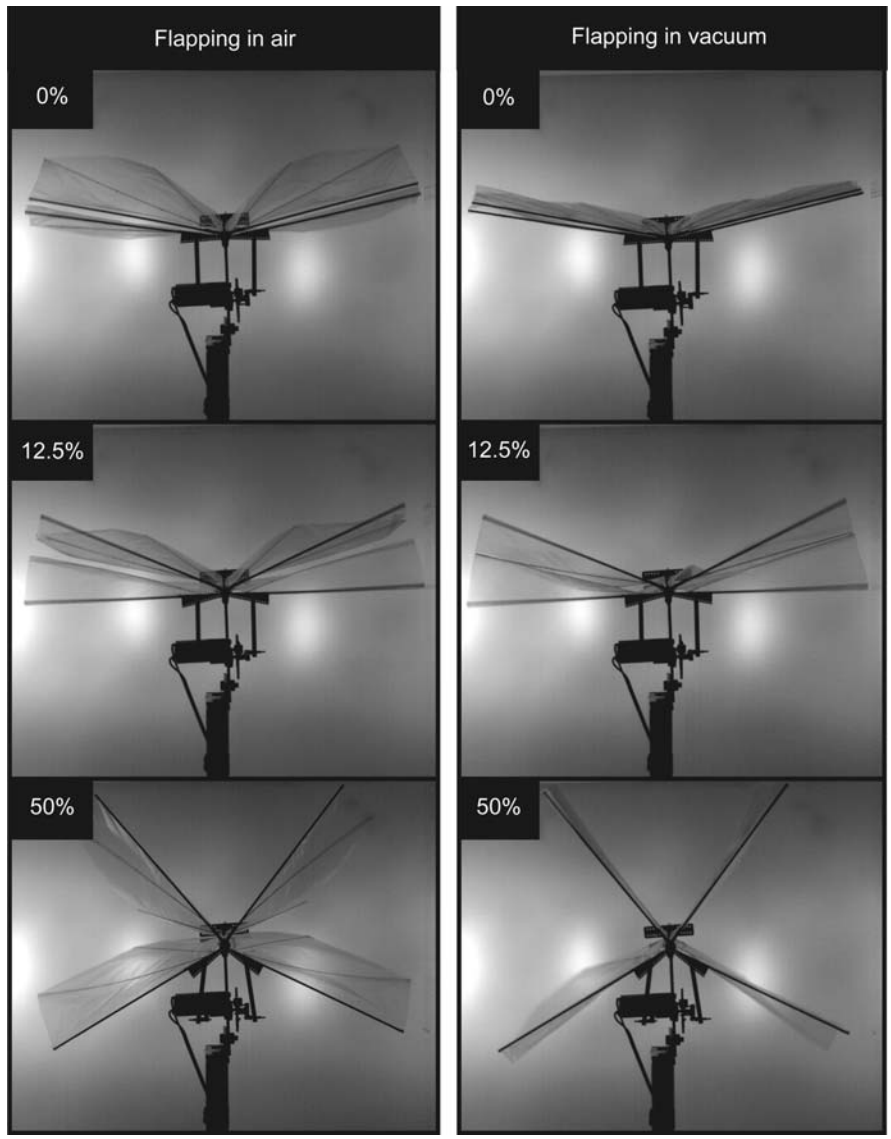

Fig. 14.19 Comparison of wing deformation under aerodynamic plus inertial wing loading in air (*left*) and inertial wing loading in vacuum (*right*) at 14 Hz and 30° flap angle. The images are snapshots at the start of the upstroke (0%), 12.5% and end (50%) of the flap cycle, where the downstroke starts. In vacuum the upper and lower foils stick together (12.5%), most likely due to electrostatic stickiness

icantly higher in air than in vacuum, hence we conclude that the aero-elastic wing deformation largely determines DelFly II's wing shape. It confirms that there is a direct coupling between wing load and the wings aerodynamic angle of attack, because the wing deforms towards lower angles of attack under loading (compare air and vacuum at 0% and 50% flap cycle). We think that the apparent wing peeling at 12.5% of the flap cycle is due to the electrostatic stickiness of the upper and lower foil. This could be tested in future studies by using non-electrostatic foils.

Based on our aerodynamic analysis we conclude that inertial and friction losses in DelFly-like designs are high and need attention. One solution could be to use elastic energy storage in a spring, tuned to the average flapping frequency of the wing. Ideally the spring has a variable stiffness such that its natural frequency continuously matches the flapping frequency.

14.7 Bio-Inspired Design of Insect-Sized Flapping Wings

Our aim is to work towards fly-sized micro-air vehicles that manoeuvre well. DelFly is still big, slow and sluggish. DelFly potentially could be controlled more directly using the flapping wings instead of the airplane tail for control. Because we focus on flapping MAVs that can actually fly, the size of every new design is limited by the smallest and lightest available components, which limits miniaturization.

A more direct approach is to start at a smaller scale and figure out how such small fly-sized flapping mechanisms, wings and actuators can be designed and constructed. This approach, pioneered in the lab of Ronald Fearing, has significantly increased our understanding of designing and building micro-flapping structures. Recently, the first wire-supported micro-mechanical insect successfully lifted off from the ground in the lab of Robert Wood [21]. Building upon the existing work in the field we wondered how we could improve the flat wing design of micro-mechanical insects and DelFly wings at the scale of insects.

The current DelFly wing is made of a D-shaped carbon fibre leading edge spar of constant thickness. A flexible Mylar foil forms the wing's surface and is stiffened by two carbon rods. The foil and carbon rods form a flat airfoil that is cambered by aerodynamic forces and, to a lesser extent, inertial forces during flapping. Aero-elastic tailoring of DelFly's wing has been done by trial and error using a strobe. At some point we even applied variable wing tension (left versus right) for thrust vectoring, but all these measures are primitive compared to the aero-elastic tailored wings of insects. Insect-sized flapping MAVs could benefit from stiffer wings for the same weight, because their shape can be controlled and tailored more directly. Wing venation, like found for insect wings, could potentially minimize or even stop wing tear, which is a problem with DelFly wings. Images of DelFly in flight often show wrinkling in trailing edges that affect its aerodynamic performance, which could be prevented by making the trailing edge stiffer. This keeps the wing foil in shape during flapping and prevents the wing from tearing. We used dragonfly wings as an inspiration to develop design principles for such stiffer micro-wings with venation-like tear-stoppers.

If we take a close look at insect wings we find that they are not flat but corrugated and wing thickness varies both span- and chord-wise. The wing structure of an insect has therefore a much richer architecture than the non-corrugated and constant thickness DelFly II wings. Compared to flat wings, corrugation improves the strength and stiffness of insect wings, because it increases the moments of area of the wing sections [16, 22, 23]. Corrugation also mediates the aero-elastic properties and vibration modes (natural frequencies) of the wing and, finally, corrugated wings are lighter for the same stiffness [16], while performing well aerodynamically [15, 16, 13, 9, 19].

We found inspiration for improving the wings of DelFly in the front wing of a dragonfly, *Sympetrum vulgatum* of the order Odonata [7]. Odonata is a primitive order of insects; their four wings possess relatively complex venation patterns. The fossil record shows that these venation patterns exist even in large dragonfly wings of up to 70 cm span, whereas current dragonflies have wing spans smaller than 10 cm, this suggests that dragonfly wings and their aerodynamic function are scalable. Although they are primitive insects, dragonflies have evolved into well-flying insects. Fast manoeuvres, silent hovering and even in-flight hunting and mating are commonly shown by these aerobatic artists. *S. vulgatum* flaps its wings at a frequency of approximately 35 Hz.

We first digitized a front wing of *S. vulgatum,* Fig. 14.20a, using a micro-CT scanner, Fig. 14.20b. The nearly 4000 cross-sectional images per wing create an accurate three-dimensional digital reconstruction of the wing. This reconstruction allowed us to quantify both the vein and shell thickness of the dragonfly wing, Fig. 14.20c1,c2. In our next step we simplified the scans by converting the wing geometry into beam and shell elements with the same geometric properties as the scan. The result is an accurate and efficient finite element model of both wings. For this dedicated processing software was written using Matlab 7.0 (MathWorks). All the elements, load data and boundaries were automatically written to an input file for Abaqus, a finite element solver for structural analysis. Using a blade element model [2], we calculated the aerodynamic and inertial loads on the wing during hovering flight, Fig. 14.20d1,d2. Using both the simplified finite element model and the calculated wing loading we determined the wings deformation, internal stresses

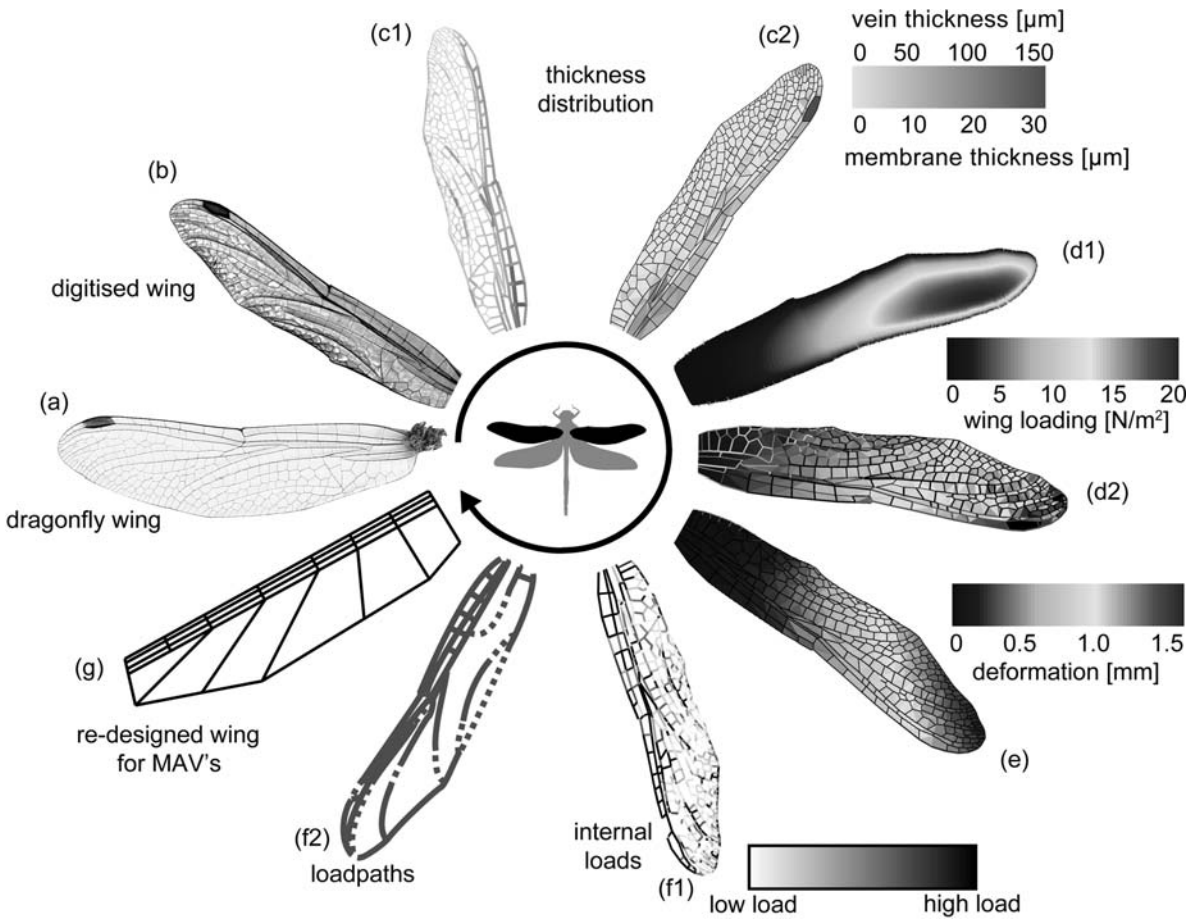

Fig. 14.20 Design wheel of an insect-sized flapping wing based on the forewing of a dragonfly (*Sympetrum vulgatum*): (**a**) original dragonfly forewing; (**b**) micro-CT scan of the dragonfly wing; (**c1**) thickness distribution of the wing veins; (**c2**) thickness distribution of the wing membranes; (**d1**) maximum aerodynamic load on the wing during hovering, computed with wing and flight data using a blade element method; (**d2**) maximum inertia loads on the wing during hovering; (**e**) maximum wing deformation during hovering; (**f1**) maximum internal loads during hovering; (**f2**) synthesized and simplified load paths in *S. vulgatum* forewing; and (**g**) the bio-inspired design of an insect-sized flapping wing

and vibration modes, Fig. 14.20e. We calculated the average load paths over a stroke cycle to estimate which veins and shells contributed most to the stiffness and strength of the wing, Fig. 14.20f1. Based on the average load paths we used engineering judgement to eliminate veins that carried only little load and connect the veins such that they formed continuous load paths, Fig. 14.20f2. In our final design step we used the simplified load paths to come up with a conceptual corrugated wing for a flapping MAV, Fig. 14.20f3 (details can be found in [7]).

The main features of the conceptual corrugated wing design are its corrugation at the leading edge. Both thickness and corrugation height decrease towards the wing tip where less stiffness is needed. Between the leading edge beams we suggest to apply ribs, to prevent the beams from buckling. Controlled buckling might be a very interesting failure mode when ultimate forces are applied on the wing. The wing design consists of several thin ribs that connect the leading and trailing edge and form 'rib-enclosed compartments' that can stop wing tearing. By carefully designing the corrugation profile, the location of supporting ribs and the thickness distribution of the 'veins', the wing can be customary tailored to perform well aero-elastically.

14.8 Production of the Bio-Inspired Wings for an Insect-Sized MAV

Although one can cut very nice two-dimensional wings out of carbon sheet using a laser cutter, this method is not well suited for building complex three-dimensional structures. We envision that a miniature three-dimensional weaving machine in combination with a mould could solve this problem [7]. Such a machine could weave carbon fibres into a three-dimensional vein network that forms the wing structure. We think an even more promising solution could be to weave thin tungsten wires and damp boron on it, a super-stiff and strong metalloid. Boron fibres are already used to stiffen the lightest planes for their size: 65 cm span at a weight of 1 g (see www.indoorduration.com). These fibres are made by vacuum coating boron on tungsten wires, hence the process is already an industry standard for making simple two-dimensional structures.

Within our project we focussed on a low-cost demonstration project using carbon fibres. We chose cyano-acrylate as a matrix for the carbon fibres, because its low viscosity results in good wetting properties of the carbon fibres. To cover the wings we chose one-sided (OS) film of 0.5 μm thickness glued with diluted Pattex (similar to DelFly wings). The wings are produced by stretching dry carbon fibres on a three-dimensional mould, Fig. 14.21. Crossing fibres are checked for sufficient contact surface between each other to ensure correct bonding. If all the dry fibres are stretched on the mould an infusion process starts by applying cyano-acrylate drops attached to the round head of a pin to the fibres. Drops of cyano-acrylate are also placed on the intersections of fibres to connect them firmly. We immediately noticed the advantage of the low-viscous cyano-acrylate; the fibres absorb the glue and spread it through the fibre by capillary force fast and easily. Pushing a pin against the fibre gives insight as to which part is sufficiently infused and which part is still dry. The wing is trimmed to its final shape after infusion and consolidation of all the fibres. Finally OS film was mounted on the carbon fibre structure using thinned glue. This process is very labour intensive, but it can be automated using a miniature three-dimensional weaving and glue machine, but even better would be to damp boron on three dimensionally woven tungsten wires.

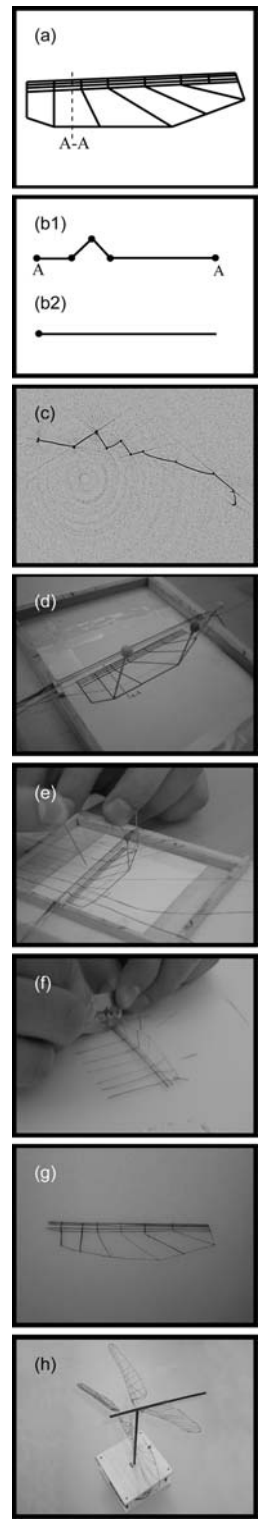

Fig. 14.21 Developing process of insect-sized flapping wings: (**a**) design of an insect-sized flapping wing inspired by a dragonfly forewing; (**b1**) cross section of re-designed wing; (**b2**) cross section of original DelFly wing; (**c**) cross section of *Sympetrum vulgatum* forewing at approximately 30% of wingspan. (**d–g**) Building method: (**d**) stretch carbon fibres on a three-dimensional mould; (**e**) consolidate structure by tipping drops of glue on the fibres with a pin; (**f**) trim consolidated wing to its final shape; (**g**) end result: insect-inspired wing made of carbon fibre. (**h**) Mock-up of future DelFly micro-equipped with wings with an advanced three-dimensional structure, which makes them stiff for their weight. Shown: tandem configuration of which the forewing and hindwing can flap 180° out of phase, like a dragon fly during slow flight

14.9 Less Is More: Spinning Is More Efficient than Flapping an Insect Wing

Having demonstrated the scalable design of flapping MAVs we conclude that the biggest challenge for fruit fly-sized air vehicles is the development of high-performance micro-components. Another challenge is energy efficiency, because existing insect size flapping MAVs are inefficient. This inefficiency is demonstrated by the low flight duration that ranges from 1 to 15 min at relatively low wing loading. The smallest mechanical insects can still not take off without power cables attached to batteries on earth. Based on aerodynamic measurements on both insect wings and DelFly II we found that the aerodynamic performance of flapping insect wings is low. We further found, similar to others [20], that simple spinning insect wings also generate a stable leading edge vortex and corresponding elevated lift and drag forces for $Re = 110$–14,000, Fig. 14.22. In fact we deliberately depicted a stable LEV on a spinning (not flapping) fruit fly wing in Fig. 14.2, because it is surprisingly similar to the one generated when the wing flaps. This observation inspired us to explicitly compare the *hover* efficacy of both flapping and spinning fruit fly wings at Reynolds numbers ranging from fruit flies ($Re = 110$) to small birds ($Re = 14{,}000$); published in Lentink and Dickinson [11], Fig. 14.23. Through this unique constant Reynolds number and equal wing shape comparison within one experiment we found that spinning insect wings outperform flapping ones up to a factor 2. This suggests that helicopter-like MAVs fitted with insect-like wings could potentially be, *up to a factor 4*, more energy efficient than flapping insect-like MAVs. Such helicopter-like MAVs can generate similarly elevated lift forces compared to flapping wings using a stable leading edge vortex. The estimated factor 4 efficiency improvement results from the combined effect

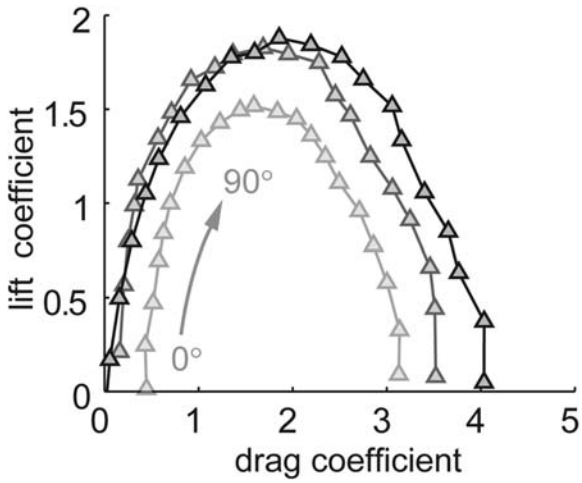

Fig. 14.22 The forces generated by a spinning fly wing depend weakly on Reynolds number. Stroke-averaged lift–drag coefficient polar of a simple spinning fruit fly wing (triangles) at $Re = 110$, 1400 and 14,000. The angle of attack (amplitude) ranges from 0° to 90° in steps of 4.5°. The lift–drag coefficient polars only weakly depend on Re, especially for angles of attack up to 45°, which correspond approximately with maximum lift. The polars at $Re = 1400$ and 14,000 are almost identical [11]

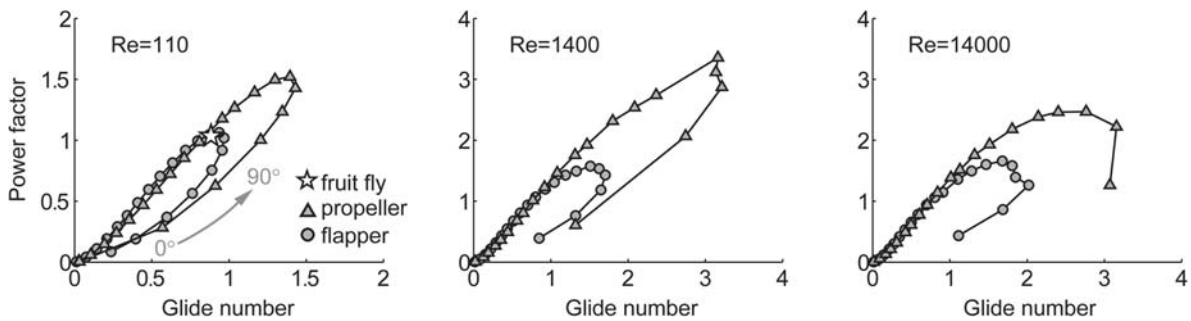

Fig. 14.23 The aerodynamic performance of a spinning fly wing is higher than that of a flapping fly wing. Stroke-averaged power factor vs. glide-number polar of a flapping versus spinning fruit fly wing at $Re = 110$, 1400 and 14,000. Aerodynamic power is proportional to the inverse of the power factor, the highest power factor represents maximum performance. These performance polars are based on the flapper data in Fig. 14.2 and the spinner data in Fig. 14.22. Note that fruit flies, at Re = 110, flap at approximately the same maximum performance level obtained with the more simple flap kinematics; they flap well (based on [11])

of a factor 2 difference in aerodynamic power and a factor 2 difference due to inertial power loss. Our study suggests, therefore, that combining both the spinning motion of helicopters and the wing shape of insects might give best of both worlds: the high lift from a stably attached leading edge vortex and the high efficiency of a spinning wing. Our study predicts therefore that a fruit fly-sized and winged air vehicle will be most efficient when fitted with spinning wings.

Acknowledgments We would like to thank the following persons and everyone else who helped us out with the research and designs presented in this chapter. **Insect flight research:** Michael Dickinson, William Dickson, Andrew Straw, Douglas Altshuler, Rosalyn Sayaman and Steven Fry at Caltech. **DelFly design:** Michel van Tooren, Rick Ruijsink, Christophe de Wagter, Bart Remes, René lagarde, Ayuel Kacgor, Wouter Roos, Kristien de Klercq, Christophe Heynze, Gijs van der Veen, Pieter Moelans, Anand Ashok, Daan van Ginneken, Michiel Straathof, Bob Mulder and Meine Oosten at TU Delft. Johan van Leeuwen at Wageningen University. Eric den Breejen, Frank van den Bogaart, Klamer Schutte, Judith Dijk and Richard den Hollander at TNO Defence, Security, and Safety. **DelFly research:** Eric Karruppannan, Evert Janssen, Jos van den Boogaart, Henk Schipper, Ulrike Müller, Gijs de Rue and Johan van Leeuwen at Wageningen University. Rick Ruijsink at TU Delft. **Insect wing research:** Elke van der Casteele at SkyScan. Adriaan Beukers at TU, Delft. Mees Muller and Johan van Leeuwen at Wageningen University.

Appendix 1 Suggested Web Sites for Ordering Micro-Components and Materials

Components/materials	Web site
Smallest RC system	www.microflierradio.com
Ornithopter kits	www.ornithopter.org
Motors, gears, etc.	www.didel.com
Micro-RC shop	www.bsdmicrorc.com
Micro-camera systems	www.misumi.com.tw
Micro-RC shop	www.plantraco.com
Miniature carbon fibre rods	www.dpp-pultrusion.com
Lightweight indoor airplanes	www.indoorduration.com
Micro-RC shop	www.peck-polymers.com
Micro-RC shop (e.g. Mylar)	www.wes-technik.de
Alternative LP batteries	www.atomicworkshop.co.uk
Rapid prototyping	www.quickparts.com

Appendix 2 Tested Parameters

Parameter	Test method
Flight speed	Measured using both a stopwatch and video-analysis of a straight flight. The flight is performed along a reference red-white tape to measure distance and climb angle. The number of video frames is also used to measure time
Flapping frequency	The flapping frequency was determined by examining audio-peaks in the audio track of the video recording. The audio file was filtered using GoldWave software
Power	The power is derived from the flapping frequency (video data) and the torque of the rubber band (torque meter in combination with counting the number of windings in the rubber band)
Rocking	Measured using video-analysis and red-white tape as a reference for rocking amplitude

References

1. Bradshaw, N.L., Lentink, D.: Aerodynamic and structural dynamic identification of a flapping wing micro air vehicle. AIAA conference, Hawaii (2008)
2. Ellington, C.P.: The aerodynamics of insect flight I-VI. Philosophical Transactions of the Royal Society of London. Series B **305**, 1–181 (1984)
3. Ellington, C.P., van den Berg, C., Willmott, A.P., Thomas, A.L.R.: Leading-edge vortices in insect flight. Nature **384**, 626–630 (1996)
4. Dickinson, M.H.: The effects of wing rotation on unsteady aerodynamic performance at low Reynolds numbers. The Journal of Experimental Biology **192**, 179–206 (1994)
5. Dickinson, M.H., Lehmann, F.O., Sane, S.P.: Wing rotation and the aerodynamic basis of insect flight. Science **284**, 1954–1960 (1999)
6. Fry, S.N., Sayaman, R., Dickinson, M.H.: The aerodynamics of free-flight maneuvers in Drosophila. Science **300**, 495–498 (2003)
7. Jongerius, S.R., Lentink, D.: Structural analysis of a dragonfly wing. Journal of Experimental Mechanics, special issue on Locomotion (2009)
8. Kawamura, Y., Souda1, S., Nishimoto, S., Ellington, C.P.: Clapping-wing Micro Air Vehicle of Insect Size. In: N. Kato, S. Kamimura (eds.) Bio-mechanisms of Swimming and Flying. Springer Verlag. (2008)
9. Kesel, A.B.: Aerodynamic characteristics of dragonfly wing sections compared with technical aerofoils. The Journal of Experimental Biology **203**, 3125–3135 (2000)
10. Lentink, D., Gerritsma, M.I.: Influence of airfoil shape on performance in insect flight. American Institute of Aeronautics and Astronautics **2003–3447** (2003)

11. Lentink, D., Dickinson, M.H.: Rotational accelerations stabilize leading edge vortices on revolving fly wings. The Journal of Experimental Biology accepted (2009)
12. Lentink, D., Dickinson, M.H.: Biofluid mechanic scaling of flapping, spinning and translating fins and wings. The Journal of Experimental Biology accepted (2009)
13. Okamoto, M., Yasuda, K., Azuma, A.: Aerodynamic characteristics of the wings and body of a dragonfly. The Journal of Experimental Biology **199**, 281–294 (1996)
14. Pornsin-Sirirak, T.N., Tai, Y.C., Ho, C.H., Keennon, M. (2001). Microbat-A Palm-Sized Electrically Powered Ornithopter. NASA/JPL Workshop on Biomorphic Robotics. Pasadena, USA
15. Rees, C.J.C.: Form and function in corrugated insect wings. Nature **256**, 200–203 (1975a)
16. Rees, C.J.C.: Aerodynamic properties of an insect wing section and a smooth aerofoil compared. Nature **258**, 141–142 (13 November 1975) doi: 10.1038/258141aO Letter (1975b)
17. Sane, S.P.: The aerodynamics of insect flight. The Journal of Experimental Biology **206**, 4191–4208 (2003)
18. Srygley, R.B., Thomas, A.L.R.: Unconventional lift-generating mechanisms in free-flying butterflies. Nature **420**, 660–664 (2002)
19. Tamai, M., Wang, Z., Rajagopalan, G., Hu, H., He, G.: Aerodynamic performance of a corrugated dragonfly airfoil compared with smooth airfoils at low Reynolds numbers. *45th AIAA Aerospace Sciences Meeting and Exhibit.* Reno, Nevada, 1–12 (2007)
20. Usherwood, J.R., Ellington, C.P.: The aerodynamics of revolving wings I-II. The Journal of Experimental Biology **205**, 1547–1576 (2002)
21. Wood, R.J.: The first takeoff of a biologically-inspired at-scale robotic insect. IEEE Trans. on Robotics **24**, 341–347 (2008)
22. Wootton, R.J.: Geometry and mechanics of insect hindwing fans: a modelling approach. Proceedings of the Royal Society of London. Series B **262**, 181–187 (1995)
23. Wootton, R.J., Herbert, R.C., Young, P.G., Evans, K.E.: Approaches to The Structural Modelling of Insect Wings. Philosophical Transactions of the Royal Society **358**, 1577–1587 (2003)